Tailoring the Morphology and Dewetting of an Organic Thin Film

J. M. Topple,* S. A. Burke,† W. Ji,‡ S. Fostner, A. Tekiel, and P. Grütter

Department of Physics, McGill University, Montreal, H3A 2T8, Canada

Received: August 12, 2010; Revised Manuscript Received: November 23, 2010

Methods of tailoring molecular thin film morphology and maturation rate were investigated by noncontact atomic force microscopy. Submonolayer coverages of 3,4,9,10-perylenetetracarboxylic diimide deposited on alkali-halides form films of needle-shaped islands, and undergo a dewetting transition when deposited on NaCl. The resulting island surface distribution, size, shape, and rate of dewetting may be varied by changing growth conditions such as temperature and by templating the substrate with single atomic layer deep pits or depositing gold nanoclusters to modify island nucleation. This characterization is an important step in controlling the structure of thin organic films for devices that are sensitive to nanoscale film structure.

Introduction

The morphology of thin films in organic electronic devices is a crucial parameter, as film structure has a strong influence on application relevant properties.[1−6] Film morphology can be controlled to some degree by growth conditions,[7,8] but post-deposition dynamic processes such as dewetting (Figure 1) and other forms of ripening can alter the film structure and resulting properties,[8−17] potentially leading to problems with device stability and functionality.

Recent interest in organic semiconductors has motivated research on a variety of organic materials for electronic and optoelectronic applications.[5,7,18,19] Perylene derivatives are one such class of organic semiconducting molecules which are easily modified,[20−29] and here we investigate the controlled growth of 3,4,9,10-perylenetetracarboxylic diimide (PTCDI). Thin films of a range of organic molecules have been studied on many different substrates (see recent reviews[2,4] and references therein). Insulating substrates provide electrical isolation for deposited structures[30] and prevent leakage currents that might otherwise hamper device characterization. Noncontact atomic force microscopy (NC-AFM) is a nondestructive, high-resolution technique ideal for imaging bulk insulator surfaces.[31−35] A variety of thin molecular films deposited on insulators have been successfully imaged using NC-AFM.[29,36−42] Such studies address the question of which structures and growth modes occur and why, prompting the next question: Can we control the result?

Controlling and tailoring the structure of organic thin films, as well as the maturation time to reach a stable device-ready film structure is a desirable ability. This study explores control over thin film morphology by adjusting growth parameters such as temperature and by varying substrate structure in three ways: templating with pits, templating with gold nanoclusters, and with use of two different alkali-halide substrates. When deposited on room temperature NaCl (001), PTCDI molecules undergo postdeposition dewetting in a dynamic process described in a previous work.[16] Heating can induce enhanced Ostwald ripening within a molecular island population. By selectively distributing nucleation sites for island growth (in Volmer−Weber thin films), the resulting film morphology and homogeneity may be altered. Alkali-halide substrates templated with monolayer deep rectangular pits (created by charge stimulated desorption of the surface prior to molecule deposition), have been used in previous studies[40,41,43,44] as traps for molecules and to promote the formation of molecular structures that may otherwise be unstable or metastable. Gold deposited on KBr has been observed to form nanoclusters[45−47] and the effect of these nanoclusters on subsequent deposition of molecules has been explored.[48,49] The structure of the interface between metal clusters and a molecular layer is of general interest for organic electronic and optoelectronic contact geometry properties.[50−52] Here the impact of templating, as well as surface structure and other growth parameters on film growth behavior and morphology are shown to provide means of tailoring of island dimensions and subsequently film continuity, homogeneity, and surface area for films of given coverages. This will consequently affect opto-electronic and other size and structure dependent properties.[1−6]

Results and Discussion

Growth on Atomically Flat Alkali-Halides. When deposited on NaCl (001) at room temperature, PTCDI molecules initially

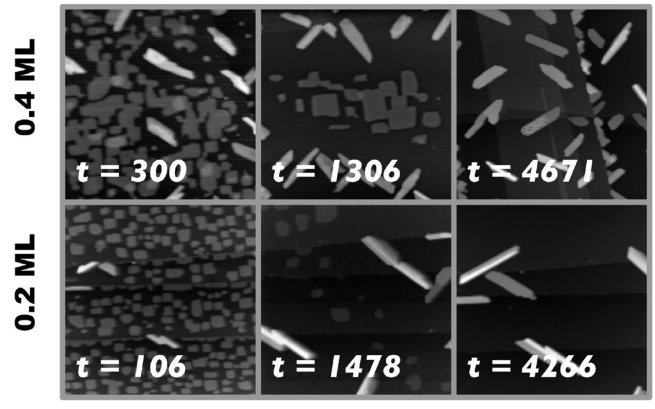

Figure 1. Dewetting of PTCDI on NaCl for two coverages with elapsed times (minutes) since deposition. All images 600 nm × 600 nm, $\Delta f =$ (top row) −3.7, −2.2, −4.0 (bottom row) −1.9, −2.4, −3.9 Hz; corresponding normalized frequency shifts $\Gamma = -0.5, -0.3, -0.6$ and $-0.3, -0.3, -0.6$ fN$\sqrt{m}$.

* To whom correspondence should be addressed. E-mail: topplej@physics.mcgill.ca.

† Also affiliated with the Department of Physics and Astrononomy and Department of Chemistry, University of British Columbia, Vancouver, V6T 1Z1, Canada.

‡ Also affiliated with the Department of Physics, Renmin University of China, Beijing 100872, China.

10.1021/jp107644u © 2011 American Chemical Society
Published on Web 12/14/2010

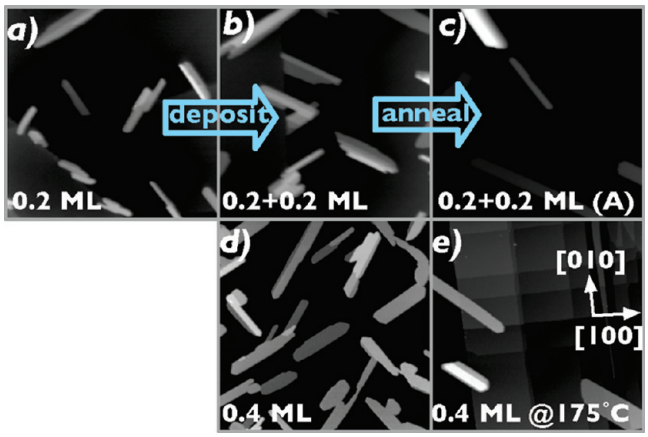

Figure 2. 600 nm × 600 nm images of PTCDI on KBr (a−d) and NaCl (e), films consisting exclusively of needle islands. (a) 0.2 ML, $\Delta f = -2.0$ Hz; $\Gamma = -0.3$, fN$\sqrt{m}$; (b) 0.4 ML deposited in 2 subsequent depositions of 0.2 ML, on the same sample show in panel a, $\Delta f = -2.8$ Hz; $\Gamma = -0.4$ fN$\sqrt{m}$; (c) the sample shown in panel b after gentle heating overnight at ∼150 °C, $\Delta f = -3.2$ Hz; $\Gamma = -0.4$ fN$\sqrt{m}$; (d) 0.4 ML deposited in a single deposition, $\Delta f = -3.1$ Hz; $\Gamma = -0.4$ fN$\sqrt{m}$; and (e) 0.2 ML PTCDI on NaCl heated to ∼175 °C during deposition; note the high step density $\Delta f = -2.0$ Hz; $\Gamma = -0.3$ fN$\sqrt{m}$.

form two coexisting island growth structures: square-shaped islands and needle-shaped islands. The metastable square islands dewet into the stable needle islands within days of deposition (see Figure 1), as escaping edge molecules diffuse away and join more energetically favorable sites. The dynamics of dewetting of PTCDI on NaCl was described in a previous work,[16] and here we explore experimental factors that can be used to control thin film morphology and enhance or inhibit dewetting.

In contrast, PTCDI deposited on KBr does not form square islands at room temperature, and has been exclusively observed to form stable needle-shaped islands similar to those found as the stable structure on NaCl (see Figure 2). KBr and NaCl share the same crystal structure, with different lattice constants of 0.660 and 0.565 nm, respectively. The molecule−substrate interaction is dominated by the electrostatic interaction between the O atoms in the C═O groups of PTCDI and Na/K cations on both substrates. The metastable square-shaped island brick-wall structure that forms on NaCl is mediated by this molecule−substrate interaction, with the intermolecular spacing corresponding to the length between two Na cations (with three lattice periods between them)[16] like the p(3 × 3) structure that is formed by a similar molecule, PTCDA when deposited on NaCl.[8] Conversely, the stable needle-shaped island structures that form on both NaCl and KBr are dominated by molecule−molecule interactions and more closely resemble the bulk crystalline structure,[16] forming canted rows due to hydrogen bonding between N−H end groups and the oxygen atoms of adjacent molecules.[26] The lack of formation of square shaped islands on KBr is likely caused by the subtle difference in substrate structure, rendering the metastable square island structure that forms on NaCl unstable and unable to form on KBr.

Needle islands on NaCl are generally two to three molecular layers taller than those grown on KBr (see Figure 6 and the Supporting Information), and are otherwise similar in appearance, size, structure and stability under high-resolution imaging conditions. The difference in height may be due to height-dependent strain,[6,53] or may be a result of the differing substrate interactions that accommodate a metastable structure only on

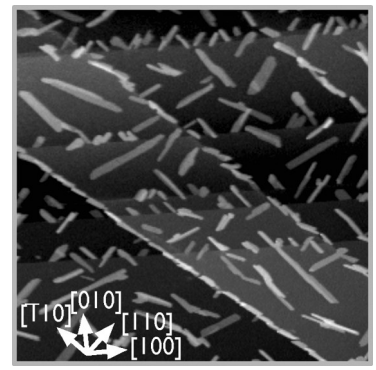

Figure 3. 1000 nm × 1000 nm image of 0.5 ML PTCDI on KBr showing needle islands nucleating from a variety of different step edges, $\Delta f = -2.0$ Hz; $\Gamma = -0.3$ fN$\sqrt{m}$.

NaCl. Additionally, needle islands on both substrates have been observed exclusively with heights of two monolayers (ML) or more. Molecule−molecule interactions appear to mediate the growth and islands form a bulk-like crystalline structure, despite the substrate lattice mismatch. The mismatch may still induce some strain, but the interface structure of a multilayer island must be determined by methods other than AFM. PTCDI films deposited on NaCl can evolve for days after deposition before producing a stable film, and needle islands are always pinned to defects. On KBr, molecules readily form needle-shaped islands with apparently less selectivity over the surface position. As a general result, shorter, more densely packed needle islands form on KBr than are observed postdewetting on NaCl for the same coverage of molecules.

Nucleation: The Importance of Defects. Needle-shaped islands of PTCDI on NaCl nucleate at defects (such as substrate step edges, kink sites, and adsorbates) and are subsequently pinned to the nucleation site,[16] similar to behavior observed by others for C_{60},[39] DiMe-PTCDI on KBr (001),[29,54] and Co-salen molecules.[17] Substrate step density has an important effect on the resulting film morphology, as needle islands tend to decorate step edges. PTCDI demonstrates interesting step preferences on both NaCl and KBr substrates, some of which may be observed in Figure 1 and Figure 3. NaCl and KBr cleave preferentially along the {100} planes to maintain charge neutrality,[55−57] and step edges in Figure 3 that appear to be along the [$\bar{1}$10] direction are probably actually composed of small ⟨100⟩ edges with kinks.[58−60] Needle-shaped islands of PTCDI on KBr are occasionally observed in the middle of terraces, but preferentially nucleate from step edges. A contrasting behavior for a similar molecule was observed by Fendrich et al., who described DiMe-PTCDI molecules deposited on NaCl and KBr to form molecular wires requiring step edges for stability on KBr, while loose ends were stable on NaCl.[29]

Double steps (two atomic layers tall) in NaCl and KBr appear to be excellent nucleation sites for needle islands, and are often nearly completely covered by smaller than average needle islands on the bottom side (see top right image in Figure 1), presumably due to enhanced interaction between the oxygen atoms of PTCDI and the second level sodium ions that become accessible and promote stacking. Needle islands nucleated at single steps often straddle both sides of the step. A single NaCl step is not tall enough for second-layer PTCDI molecules to reach the NaCl atoms (with a step height of 0.283 nm versus island layer height of ∼0.315 nm[16,21]), thus the lack of sodium ion interaction for second level molecules may account for the reduced density of needle islands nucleated at single step edges. The long axis of molecular islands are often approximately

parallel to the ⟨110⟩ directions of the substrate. Islands tend to grow following the double step edges if the steps are approximately along the ⟨110⟩ directions of the substrate (see Figure 3), while steps approximately along the ⟨100⟩ directions of the substrate tend to nucleate islands that do not follow the step edge and have shorter than average length. Gold clusters and other adsorbates in general are less selective and tend to decorate any step edge, and can subsequently nucleate PTCDI needle island growth.

Making Islands Larger. ***Additional Deposition.*** Additional molecules may be deposited onto a stable film to increase molecular island size without drastically changing the distribution of islands over the surface. PTCDI (0.2 ML) was deposited on KBr to produce a stable film, the film was imaged (Figure 2a), and then an additional 0.2 ML was deposited the next day (Figure 2b). A single deposition of 0.4 ML is show for comparison in Figure 2d (and see Figure 6 and Supporting Information for resulting island dimensions). The film produced after the second deposition of 0.2 ML (Figure 2b) contained islands that were longer, wider but similar in height and surface distribution to those observed after the initial 0.2 ML deposition (Figure 2a). Analysis of several images suggests that molecules of the second deposition generally join existing layers of islands without nucleating new islands or layers. It is reasonable to assume that the edges of previously established islands provide the most energetically favorable binding sites. When compared to a single deposition of 0.4 ML (Figure 2d), the doubly deposited film contained islands which were again longer, wider, and similar in height, yet the doubly deposited islands had a larger interisland spacing (note that the substrate step density plays a role in dictating the island surface distribution and dimensions, and will be discussed further below). Therefore, it appears possible to set the island surface distribution with an initial deposition, and then increase the island size with subsequent depositions.

Heating. Heating of a stable film after growth (annealing) can be used to induce Ostwald ripening and increase the size of compact islands while thinning out the distribution of islands over the surface. The KBr sample discussed above (Figure 2a,b) was subsequently annealed at ∼150 °C overnight. After annealing (Figure 2c), the islands observed were longer, spread farther apart, and many were significantly taller than those observed prior to heating. The tallest island observed was 13 nm tall, corresponding to a height of about 40 molecular layers. Alternatively, a sample may be heated during molecule deposition to influence growth in a similar way, again resulting in larger islands. Deposition onto a warm NaCl substrate (∼175 °C, Figure 2e) exclusively produces large needle-shaped islands comparable in size to those grown on KBr (Figure 2c). The measured island dimension distributions are illustrated in Figure 6 (see also Supporting Information), although difficulties in finding and imaging such large islands resulted in a small number of islands from which to take statistics. Branched islands indicative of coalescence were rarely seen for the postdeposition annealing on KBr case (Figure 2c) and were never observed on NaCl heated during deposition (Figure 2e). This, combined with the larger interisland spacing and bare step edges that are typically decorated during room temperature deposition, indicates higher mobility of the molecules. Similar observations have been made as a result of annealing for many systems.[8−11,13,15] Heating is a means of increasing the average island size (particularly height)[8] and interisland spacing, thereby tailoring the morphology of the resulting thin film.

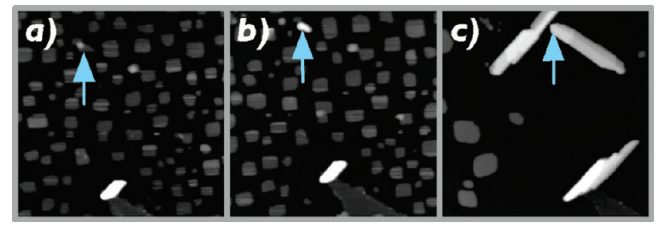

Figure 4. 500 nm × 500 nm images of 0.2 ML PTCDI on NaCl (a) with a single needle-shaped island visible (and some unstable second layers on square islands) 203 min after deposition, (b) newly nucleated needle-shaped islands immediately after poke, 254 min after deposition, and (c) needle-shaped islands 2227 min after deposition. Arrow indicates indent location. $\Delta f = -3.8$, -4.0, and -4.3 Hz; $\Gamma = -0.5$, -0.6, and -0.6 fN$\sqrt{m}$.

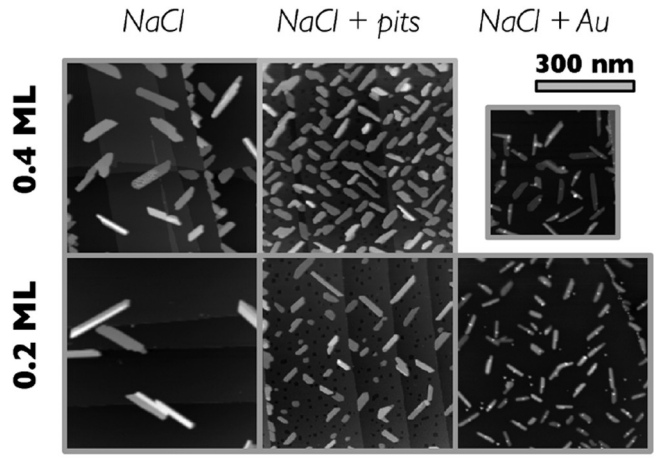

Figure 5. Changes in resulting film morphology with varying substrate structure. NC-AFM images of two coverages of PTCDI deposited on NaCl, Δf = (top row) -4.0, -3.0, -4.6 (bottom row) -3.9, -2.0, -2.0 Hz; $\Gamma = -0.6$, -0.4, -0.6 and -0.6, -0.3, -0.3 fN$\sqrt{m}$.

Making Islands Smaller. ***Tip Induced Nucleation.*** It is possible to induce site-specific nucleation by poking the sample with the AFM tip during dewetting to create a local defect, as illustrated in Figure 4 (see Supporting Information for movie). Needle island growth was nucleated at a position where the AFM tip interacted with the surface, producing a small local rearrangement or indentation. This method allows for precise positioning of defects over a small range accessible by imaging, but control over a large scale is desirable for thin film device applications.

Pits. The importance of step density lends itself to the notion that control over the density of nucleation sites can be achieved by careful modification of the surface. Monolayer deep rectangular pits in the NaCl substrate provide a relatively homogeneous surface distribution of kink sites over the surface, which can nucleate needle-shaped islands, as shown in Figure 5). Pits can also act as traps for PTCDI molecules, and occasionally small, single layer islands of trapped molecules form that fill the square-shaped pit and are the only monolayer structures that are stable over long times. A comparison of dimensions for postdewetting needle-shaped islands for varying substrate structures is given in Figure 6. Complete dewetting of the square islands occurs very quickly, within an hour of PTCDI deposition, whereas untemplated (unaltered) samples may take in excess of 50 h to completely dewet. The resulting needle islands tend to be about a factor of 10 smaller in volume and somewhat less elongated (aspect ratios of ∼2.5:1 compared to ∼4:1) than those for the same coverage on unaltered NaCl (see Supporting Information for more images). The size and density of pits (and

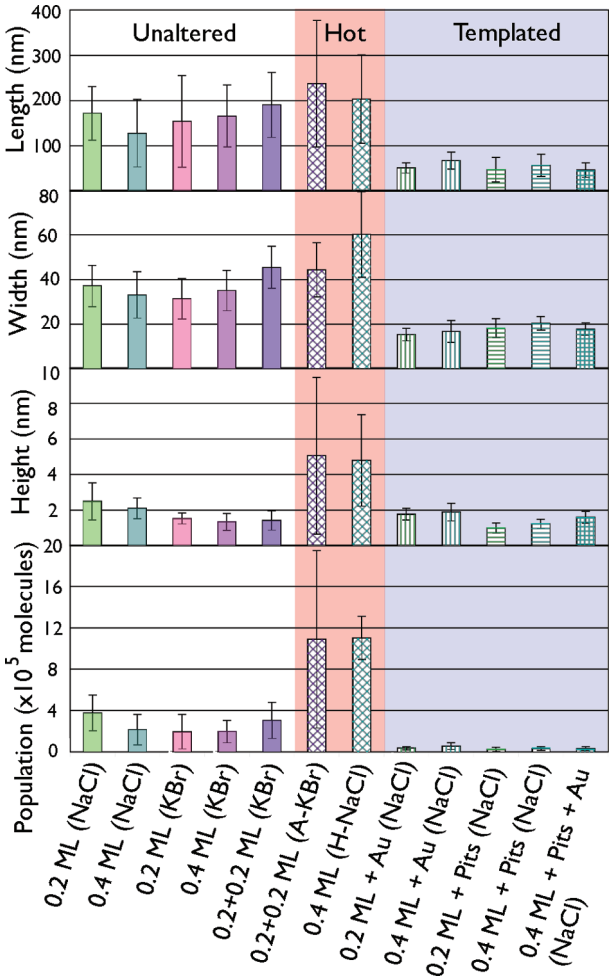

Figure 6. Postdewetting needle island average length, width, height, and population per island with standard deviations for varying coverages and substrate structures. Standard deviations are indicative of broad distributions from variation between islands, not measurement uncertainty. Uncertainty on individual island measurements generally ranges from approximately 3% for large islands to 12% for small islands."A-" and "H-" indicate samples that were annealed after growth or heated during molecule deposition, respectively.

thus the separation and density of kinks) can be controlled by varying temperature and charge dose.[64] However, double-layer step edges are still favored as nucleation sites even over the pits. Thus, it is impossible to create a totally homogeneous surface distribution on a typical NaCl sample (which contains many steps).

The epitaxy of all PTCDI structures observed herein are shown in Figure 7. Pit-trapped islands have the same structure as the metastable square-shaped islands observed previously on unaltered NaCl. Both form single monolayer (2×2) brick wall structures with all molecules in equivalent positions with respect to the NaCl substrate (Figure 7d,g), in contrast with the characteristic canted row structure observed in the needle-shaped islands (Figure 7e,f,h,i) and on a variety of other substrates.[20−28] The crystalline structures of the monolayer square island and multilayer needle islands PTCDI on NaCl were determined in a previous work.[16] All lattice constants are given in Table 1, determined from atomic and molecular resolution images such as Figure 7f and the well-known lattice constants of NaCl and KBr.

In both pit-trapped and square-shaped islands, the molecule−substrate interaction appears to influence growth sufficiently to hold a single monolayer of molecules to the preferred adsorption sites, the same sites preferred for PTCDA on NaCl calculated by Ji et al.[8,30] PTCDA molecules trapped in pits have been observed with a strained 2×4 herringbone-like structure and a variety of structural defects, which exhibit different optoelectronic properties depending on structure.[44] PTCDI molecules appear to fill pits more uniformly (defects have only been observed in corners) and should therefore produce a narrower range of electronic properties.

Although pit-trapped islands and square-shaped islands in the middle of terraces have the same structure, pit-trapped structures are probed more easily, which we attribute to the added stability arising from the pit edges.[41,43] The pit edges likely offer an additional edge-molecule interaction that strengthens the molecule−surface interaction, giving rise to higher diffusion and dewetting barriers (the dewetting barrier is the energetic barrier arising from the change in PTCDI configuration during the transition from the square island structure to the needle island structure). The brick-wall structured islands are less stable than the needle islands, but needle islands require a defect to nucleate and are pinned to the site.[16] Brick-wall structure filled pits have been observed as long as 10086 min (8 days) after deposition. A higher dewetting barrier may partially explain the long life of these filled pits; despite the presence of kink sites at pit corners, a higher dewetting barrier would delay the nucleation of needle islands. It is possible to disturb square islands by imaging with a frequency shift on the order of −10 Hz (corresponding to a normalized frequency shift of ~ -1.4 fN$\sqrt{m}$), pit-trapped structures may be disrupted by imaging with frequency shifts in excess of −25 Hz, while needle islands are stable in excess of −30 Hz (corresponding normalized frequency shifts of ~ -3.5 and -4.3 fN$\sqrt{m}$ respectively). Comparatively, Kawai et al. observed cutting of meso-(4-cyanophenyl)-substituted Zn(II) porphyrin molecular wires self-assembled on KBr(001) (nucleated from step edges and gold nanoclusters) at -3.6 fN$\sqrt{m}$, and noted that the molecules were weakly bound to both the substrate and the rest of the wire.[65]

Gold. Gold nanoclusters tend to decorate steps in the NaCl, although some still form in the middle of terraces, similar to gold deposited on KBr.[46−49,65,66] Like the pits, gold clusters also act as nucleation sites for needle islands and dewetting is completed within about 5 h (see supplementary info). Resulting islands tend to be similar in length to those formed by the same coverage of PTCDI on pit-templated NaCl, but are ∼15% narrower and nearly twice as tall, as can be seen in Figure 5 and Figure 6.

The affinity of PTCDI to nucleate from gold promotes it as a promising electrical contact material for organic electronics. Because the gold nanoclusters are not quasi-two-dimensional like the pits (and steps), the islands on gold-templated samples may be modulated by the dimensions of the gold clusters, which are generally taller and narrower than pits. PTCDI molecules typically extend from both sides of the gold, with the gold nanocluster in the middle of the needle-shaped island, in contrast to cyanoporphyrin wires grown on Au decorated KBr observed by the group of Glatzel and Kawai et al.[49,65] The gold seems to decrease the tendency of needle islands to grow in width, promoting interlayer mass transport and the formation of upper layers. Zhong et al. modeled the efficient ascending interlayer transport of oligoethylene-bridged diferrocene molecules on Ag(110), which form mesalike islands in what they describe as a strain-driven ascending process, preferentially attaching to upper unstrained layers with higher effective binding energies than strained layers close to the substrate.[53]

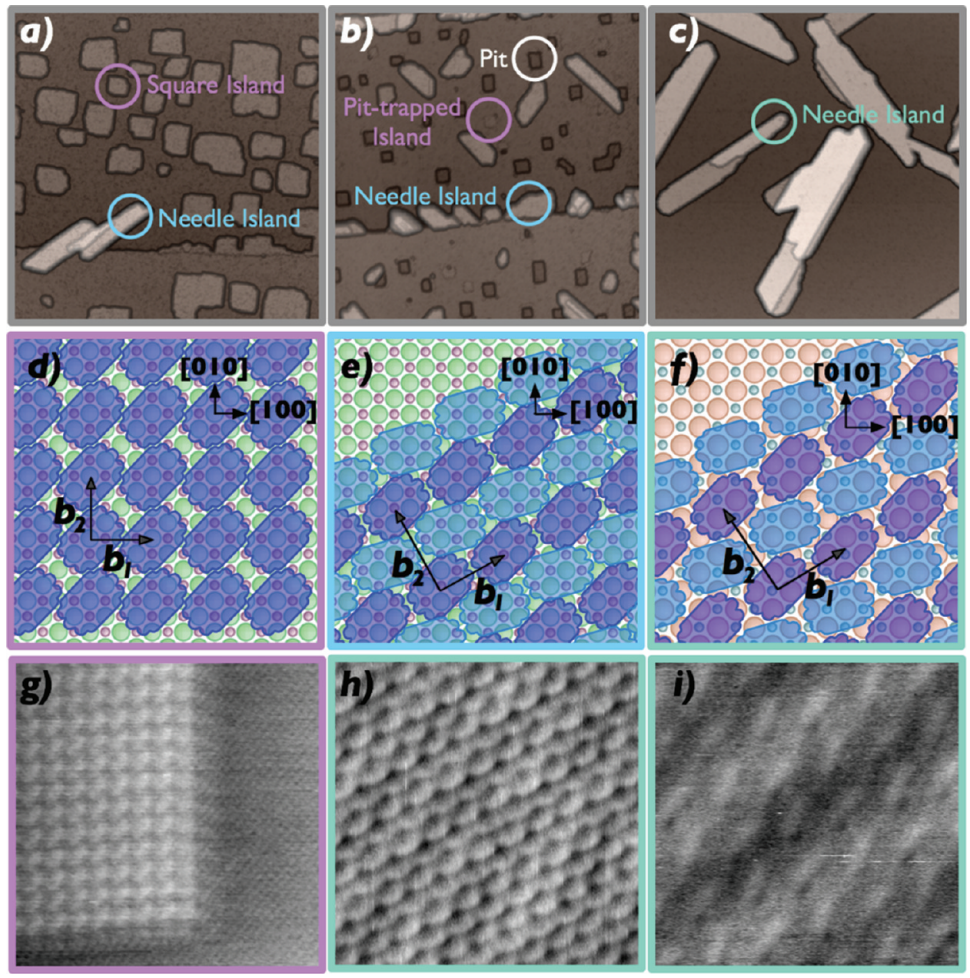

Figure 7. Epitaxy of PTCDI on NaCl and KBr. (Top row) 300 nm × 300 nm images of (a,b) 0.2 ML deposited on flat and pit-templated NaCl, (c) 0.4 ML deposited on KBr, three-dimensionally rendered to enhance pit visibility. $\Delta f = -4.0, -2.2, -2.3$ Hz; $\Gamma = -0.6, -0.3, -0.3$ fN$\sqrt{m}$. Middle row: Illustrations of (d) (2 × 2) brick wall structure of both square island and pit-trapped molecules on NaCl, (e,f) needle island structure observed on NaCl and KBr, respectively (top layer of molecules only shown for clarity). Bottom row: (g) 15 nm × 15 nm image of molecules trapped in a pit with surrounding NaCl lattice, (h,i) 10 nm × 10 and 5 nm × 5 nm images illustrating needle-island structure of PTCDI on KBr. $\Delta f = -6.0, -14.8, -17.4$ Hz; $\Gamma = -0.8, -2.1, -2.5$ fN$\sqrt{m}$.

TABLE 1: Needle, Square, and Pit Lattice Constants

structure	b_1 (nm)	b_2 (nm)	θ (°)	β (°)
needle (NaCl)	1.32 ± 0.03	1.65 ± 0.04	29 ± 1	90 ± 2
needle (KBr)	1.42 ± 0.02	1.75 ± 0.05	29 ± 1	93 ± 3
square (NaCl)	1.13 ± 0.04	1.09 ± 0.08	1 ± 3	93 ± 4
pit (NaCl)	1.15 ± 0.04	1.14 ± 0.04	1 ± 1	88 ± 2
preferred NaCl sites	1.13	1.13	0	90

Pits + Gold. Combining the two templating methods is a promising means of creating controlled nanoscale hybrid molecule-metal structures,[48] and also results in a more homogeneous surface distribution of gold nanoclusters over the surface (see Supporting Information for images). Pits were created initially, followed by deposition of 0.05 nm of gold and then 0.4 ML of PTCDI, similar to previous experiments done by Mativetsky et al. with PTCDA molecules deposited on KBr.[48] The resulting film exhibited rapid dewetting, which was complete within an hour, and had intermediate needle island dimensions given in Figure 6 (see also Supporting Information).

General Discussion

Nucleation Site Growth Dependence. ***Comparison of Morphologies.*** In general, templated surfaces contain more nucleation sites than unaltered surfaces, and can produce many small needle-shaped islands close together (presuming negligible Ostwald ripening, see Figure 6 and Supporting Information). The dimensions of needle-shaped islands also depend on the coverage of molecules deposited. In general, more molecules for the same surface preparation results in larger islands (this is true only if the nucleation site surface distribution is kept constant. A higher step density produces smaller islands in the top left image of Figure 5). Unaltered NaCl and KBr are easily cleaved to produce atomically flat terraces on the order of micrometers in size, resulting in fewer nucleation sites and therefore larger, more spread out needle islands. PTCDI islands grown on unaltered substrates tend to be about 3 times the length and an order of magnitude larger in volume than those of the same coverage grown on templated substrates. The size of the needle-shaped islands produced in a film depends on the density of nucleation sites, and the lack of control over the positioning of step edges of alkali-halide surfaces results in a large variation of molecular island size (standard deviation of ∼50% in volume) and surface distribution (double step edges are densely decorated) when grown on unaltered substrates. Also, islands grown on gold-templated NaCl substrates tend to be about twice the height and ∼15% narrower than those grown on pit-templated substrates for the same coverage of molecules deposited. While the reason for this difference in geometry is

not well understood, it appears that the islands are modulated by the dimensions of the gold clusters.

Contaminants as Nucleation Sites. It should be noted that while this study includes samples prepared exclusively under UHV, the environment is expected to play a crucial role in film structure. Contaminants may act as nucleation sites, diffusion barriers, surfactants, strain reducers, and create defects. Atomic steps and kink sites are well-known as traps for contaminants[61−63] due to their lower coordination numbers, which may in turn nucleate needle island growth[39] and suppress the formation of metastable structures.

Molecular Behavior. ***Diffusion.*** By providing more nucleation sites, it is possible to create a higher surface density of smaller islands, but one must also consider the dynamics of the growth process. PTCDI molecules are capable of diffusing long distances (on the order of hundreds of nanometers) before binding to a stable site (see, for example, Figures 4 and 5) as films evolve over the course of days at room temperature, and at elevated temperatures may travel even farther and over higher energy barriers (such as steps). The relatively low diffusion barriers for single PTCDI molecules diffusing between adjacent preferred adsorption sites on NaCl at room temperature have been calculated using density functional theory (see Supporting Information for details) to be 0.41 and 0.27 eV along and perpendicular to the long molecular axis, respectively. Diffusion barriers and travel distances play an important role in the resulting film morphology.[16] In the dewetting scenario, needle-shaped islands are populated by molecules escaping from the surrounding metastable square-shaped islands. Even with negligible Ostwald ripening between needle-shaped islands, there is competition for the capture of free molecules diffusing from the square-shaped islands. If more needle-shaped islands nucleate, diffusing molecules travel smaller distances before being trapped, resulting in faster dewetting, smaller needle-shaped islands and a more homogeneous distribution of islands over the surface. Smaller molecule travel distances require shorter transit time, thus templated films exhibit faster dewetting, producing stable films within a matter of hours instead of days at room temperature.

Anisotropic Growth. We speculate that a diffusing molecule incident on the side of a needle island may hop along the side of an unfavorable edge until it reaches a location with sufficient stability to attach, similar to adatom behavior in the atomistic compact island growth regime.[61] Given the tendency of PTCDI molecules to join end-to-end,[16,26] needle islands tend to elongate with time. This behavior is akin to the more pronounced anisotropic growth of wirelike islands of DiMe-PTCDI on KBr and NaCl (001),[29] and exploited by Kawai et al. for "self-healing" meso-(4-cyanophenyl)-substituted Zn(II) porphyrin molecular wires.[65] The end-to-end intermolecular interaction is due to the hydrogen bonding between N−H and C═O groups, so growth occurs preferentially from the ends of islands as existing rows tend to elongate over the formation of new adjacent rows.

Suppression. If a PTCDI needle island extends during growth toward an adjacent island with a different orientation (as may be the case more frequently for higher coverages), the islands may coalesce, or if coalescence is unfavorable, the growth in this direction may be suppressed (see Figure 4 and Supporting Information for movie). If suppressed, molecules diffusing along the island sides with insufficient coordination to attach would be unable to further elongate the island in that direction, and may continue to diffuse until eventually either reaching a different favorable location or being joined by other molecules to form a new row and thus widen the island. Such suppression may occur more frequently for samples with high nucleation site density and relatively short island heights at a given coverage, such as the pit-templated case in Figure 5. In such instances, the surface area covered by islands may be sufficiently high that island dimensions are not dictated by competitive dewetting and substrate structure alone, and suppression may arise where many needle-shaped islands with differing orientations grow in close proximity to one another. This suppression is exemplified in Figure 8, showing two subsequent 1 ML depositions of PTCDI on KBr. After the second deposition, the closely packed needle-shaped islands maintain similar island surface distributions due to suppression, and increase from 1.1 ± 0.2 nm to 1.7 ± 0.5 in average height (partial coalescence creates ambiguity in determining other island dimensions). This procedure is akin to templating in that the island surface distribution is set by an initial deposition, but in this case, existing island edges generally act as the most stable binding site for additional molecules, providing another means of tailoring the resulting thin film morphology.

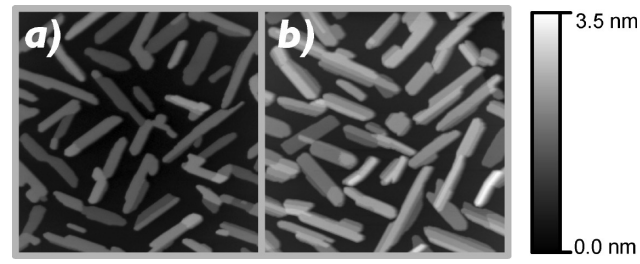

Figure 8. 600 nm × 600 nm images of subsequent depositions of PTCDI on KBr, illustrating suppression (a) 1 ML, average island height 1.1 ± 0.2, $\Delta f = -2.0$ Hz; $\Gamma = -0.3$ fN$\sqrt{m}$ and (b) 2 ML, average island height 1.7 ± 0.5 nm $\Delta f = -2.9$ Hz; $\Gamma = -0.4$ fN$\sqrt{m}$.

Conclusion

Growth conditions and surface structuring can provide a means of control over organic thin film morphology, which should lead to controllable device relevant properties. The electronic properties of molecular islands are determined by structure, and are key to the performance of potential molecular devices. For example, needle-shaped and square islands should offer different charge carrier mobilities owing to the different intermolecular orientations resulting in different wave function overlap. Defects and grain boundaries may lead to a change in the resistivity of islands and thin films. The influence of experimental factors on the morphology of PTCDI thin films was investigated, and parameters were identified that may be varied to induce desired behavior and produce tailored film morphologies. Two methods of increasing stable needle island size were explored. Two-step depositions can be used to increase the average needle island size without changing the distribution of islands on the surface, producing a more dense island surface distribution than is accessible by a single deposition. Heat can be applied either during molecule deposition or afterward (annealing) to increase the kinetic energy of molecules and enhance ripening, producing larger islands distributed more sparsely over the surface. Defects act as island nucleation sites and play a crucial role in determining film structure. Templating a surface with monolayer deep pits or gold nanoclusters can increase the nucleation site density and tailor the size, shape, surface distribution, and dewetting time of needle-shaped PTCDI islands nucleated on NaCl. To gain a microscopic picture of how these "tuning knobs" influence large anisotropic molecules

on surfaces, there is a need for comparative modeling, such as within a kinetic Monte Carlo framework.[53,67,68] However, the experiments shown here demonstrate some of the methods that can be applied to modify the final stable film morphology including and even exploiting the effects of dewetting. The ability to control molecular film morphology through substrate modification, especially where dewetting occurs, is a general concept and may prove useful in the context of dialing in thin film properties for devices.

Experimental Section

Preparation and characterization of samples took place in the JEOL JSPM 4500A Ultra-High Vacuum (UHV) AFM system. Single crystal NaCl (Korth Kristalle, Germany) samples were cleaved in situ and heated to ~150 °C for 1 h. Pits were created by irradiating the surface with charge using an electron beam evaporator (Oxford Applied Research) below the evaporation threshold, at a sample temperature of ~250 °C with a charge dose of 1.2 ± 0.1 μC/cm^2. The details of pit creation are described elsewhere.[6,40] Gold was deposited using the same evaporator, at a coverage of 0.005 nm for all samples shown. A molecular evaporator (Kentax) was used to thermally evaporate PTCDI (Alfa Aesar, 98% purity, outgassed at 200 °C overnight) at 300 °C onto room temperature substrates. Deposition rates were calibrated (assuming densities of 1.7 g/cm^2 for PTCDI and 19.3 g/cm^2 for gold) using a quartz crystal microbalance (Inficon). Molecule deposition rates ranged from 48 to 96 pm/min, and gold was deposited at 7−15 pm/min. Samples were subsequently imaged by NC-AFM using a modified Nanosurf easyPLL (phase-locked loop), with constant oscillation amplitudes of 6−7 nm in constant frequency shift topography mode. Nanosensors cantilevers (PPP-NCLR) with typical resonance frequencies of 160−170 kHz and spring constants of ~40 N/m were used.

Acknowledgment. The authors thank Roland Bennewitz for helpful discussion of alkali halide steps and facets, Lynda Cockins for insight and advice, and the following funding agencies: NSERC, CFI, FQRNT, CIfAR and the Walter Sumner Foundation.

Supporting Information Available: Experimental details and additional figures relating to substrate preparation, characterization of pit-templated and pits-plus-gold-templated samples, needle island morphology and diffusion modeling. This material is available free of charge via the Internet at http://pubs.acs.org/.

References and Notes

(1) Schouwink, P.; Schäfer, A. H.; Seidel, C.; Fuchs, H. *Thin Solid Films* **2000**, *372*, 163–168.
(2) Hooks, D. E.; Fritz, T.; Ward, M. D. *Adv. Mater.* **2001**, *13*, 227.
(3) Tanaka, K.; Fujita, S. *Proceedings 7th Int. Conf. Prop. Appl. Dielectr. Mater. (Cat. No.03CH37417)* **2003**, 45–48.
(4) Witte, G.; Woll, C. *J. Mater. Res.* **2004**, *19*, 1889–1916.
(5) Barth, J. V.; Costantini, G.; Kern, K. *Nature* **2005**, *437*, 671–679.
(6) Burke, S. A.; LeDue, J. M.; Miyahara, Y.; Topple, J. M.; Fostner, S.; Grutter, P. *Nanotechnology* **2009**, *20*, 264012.
(7) Horowitz, G. *Adv. Mater.* **1998**, *10*, 365–377.
(8) Burke, S. A.; Ji, W.; Mativetsky, J. M.; Topple, J. M.; Fostner, S.; Gao, H.-J.; Guo, H.; Grtter, P. *Phys. Rev. Lett.* **2008**, *100*, 186104.
(9) Wan, K. J.; Lin, X. F.; Nogami, J. *Phys. Rev. B* **1993**, *47*, 13700–13712.
(10) Thürmer, K.; Williams, E. D.; Reutt-Robey, J. E. *Phys. Rev. B* **2003**, *68*, 155423.
(11) Krause, B.; Dürr, A. C.; Schreiber, F.; Dosch, H.; Seeck, O. H. *J. Chem. Phys.* **2003**, *119*, 3429–3435.
(12) Williams, E. D. *MRS Bull.* **2004**, *29*, 621–629.
(13) Silly, F.; Castell, M. R. *Phys. Rev. Lett.* **2006**, *96*, 086104.
(14) Burke, S. A.; Mativetsky, J. M.; Fostner, S.; Grtter, P. *Phys. Rev. B* **2007**, *76*, 035419.
(15) Dienel, T.; Loppacher, C.; Mannsfeld, S. C. B.; Forker, R.; Fritz, T. *Adv. Mater.* **2008**, *20*, 959.
(16) Topple, J. M.; Burke, S. A.; Fostner, S.; Grütter, P. *Phys. Rev. B* **2009**, *79*, 205414.
(17) Fremy, S.; Schwarz, A.; Lammle, K.; Prosenc, M.; Wiesendanger, R. *Nanotechnology* **2009**, *20*, 405608.
(18) Dimitrakopoulos, C. D.; Malenfant, P. R. L. *Adv. Mater.* **2002**, *14*, 99.
(19) Forrest, S. R. *Nature* **2004**, *428*, 911–8.
(20) Ludwig, C.; Gompf, B.; Petersen, J.; Strohmaier, R.; Eisenmenger, W. *Z. Phys. B - Condens. Matter* **1994**, *93*, 365–373.
(21) Kazmaier, P. M.; Hoffmann, R. *J. Am. Chem. Soc.* **1994**, *116*, 9684–9691.
(22) Klebe, G. Data deposited at the Cambridge Crystallographic Data center (CCDC), File CIF_LENPEZ, CSD No 55462, 1994.
(23) Uder, B.; Ludwig, C.; Petersen, J.; Gompf, B.; Eisenmenger, W. *Z. Phys. B - Condens. Matter* **1995**, *97*, 389–390.
(24) Tojo, K.; Mizuguchi, J. *Z. Kristallogr.- New Cryst. Struct.* **2002**, *217*, 517–518.
(25) Guillermet, O.; Glachant, A.; Hoarau, J. Y.; Mossoyan, J. C.; Mossoyan, M. *Surf. Sci.* **2004**, *548*, 129–137.
(26) Swarbrick, J. C.; Ma, J.; Theobald, J. A.; Oxtoby, N. S.; O'Shea, J. N.; Champness, N. R.; Beton, P. H. *J. Phys. Chem. B* **2005**, *109*, 12167–12174.
(27) Kunstmann, T.; Schlarb, A.; Fendrich, M.; Wagner, T.; Mller, R.; Hoffmann, R. *Phys. Rev. B* **2005**, *71*, 121403.
(28) Guillermet, O.; Glachant, A.; Mossoyan, M.; Mossoyan, J. C. *J. Phys. IV* **2006**, *132*, 77–81.
(29) Fendrich, M.; Lange, M.; Weiss, C.; Kunstmann, T.; Möller, R. *J. Appl. Phys.* **2009**, *105*, 094311.
(30) Ji, W.; Burke, S.; Gao, H.-J.; Grutter, P.; Guo, H. Unpublished work, 2008.
(31) Albrecht, T. R.; Grutter, P.; Horne, D.; Rugar, D. *J. Appl. Phys.* **1991**, *69*, 668–673.
(32) Reichling, M.; Barth, C. *Phys. Rev. Lett.* **1999**, *83*, 768–771.
(33) Barth, C.; Reichling, M. *Nature* **2001**, *414*, 54–7.
(34) Morita, S.; Wiesendanger, R.; Meyer, E. *Noncontact Atomic Force Microscopy: Nanoscience and Technology*; Morita, S., Wiesendanger, R., Meyer, E., Eds.; Springer: Berlin/New York, 2002; Vol 2 (includes bibliographical references and index).
(35) Ashworth, T. V.; Pang, C. L.; Wincott, P. L.; Vaughan, D. J.; Thornton, G. *Appl. Surf. Sci.* **2003**, *210*, 2–5.
(36) Fukuma, T.; Kobayashi, K.; Noda, K.; Ishida, K.; Horiuchi, T.; Yamada, H.; Matsushige, K. *Surf. Sci.* **2002**, *516*, 103–108.
(37) Sasahara, A.; Uetsuka, H.; aki Ishibashi, T.; Onishi, H. *Appl. Surf. Sci.* **2002**, *188*, 265–271.
(38) Nony, L.; Bennewitz, R.; Pfeiffer, O.; Gnecco, E.; Baratoff, A.; Meyer, E.; Eguchi, T.; Gourdon, A.; Joachim, C. *Nanotechnology* **2004**, *15*, S91–S96.
(39) Burke, S. A.; Mativetsky, J. M.; Hoffmann, R.; Grtter, P. *Phys. Rev. Lett.* **2005**, *94*, 096102.
(40) Mativetsky, J. M.; Burke, S. A.; Fostner, S.; Grutter, P. *Nanotechnology* **2007**, *18*, 105303.
(41) Pakarinen, O. H.; Mativetsky, J. M.; Gulans, A.; Puska, M. J.; Foster, A. S.; Grutter, P. *Phys. Rev. B* **2009**, *80*, 085401.
(42) Rahe, P.; Nimmrich, M.; Greuling, A.; Schtte, J.; Stara, I. G.; Rybacek, J.; Huerta-Angeles, G.; Stary, I.; Rohlfing, M.; Khnle, A. *J. Phys. Chem. C* **2009**, *114*, 1547–1552.
(43) Nony, L.; Gnecco, E.; Baratoff, A.; Alkauskas, A.; Bennewitz, R.; Pfeiffer, O.; Maier, S.; Wetzel, a.; Meyer, E.; Gerber, C. *Nano Lett.* **2004**, *4*, 2185–2189.
(44) Burke, S. A.; LeDue, J. M.; Topple, J. M.; Fostner, S.; Grütter, P. *Adv. Mater.* **2009**, *21*, 2029–2033.
(45) Goryl, M.; Buatier de Mongeot, F.; Krok, F.; Vevecka-Priftaj, A.; Szymonski, M. *Phys. Rev. B* **2007**, *76*, 075423.
(46) Mativetsky, J. M.; Fostner, S.; Burke, S. A.; Grutter, P. *Surf. Sci.* **2008**, *602*, L21–L24.
(47) Mativetsky, J. M.; Fostner, S.; Burke, S. A.; Grutter, P. *Phys. Rev. B* **2009**, *80*, 045430.
(48) Mativetsky, J. M.; Burke, S. A.; Fostner, S.; Grutter, P. *Small (Weinheim an der Bergstrasse, Germany)* **2007**, *3*, 818–21.
(49) Glatzel, T.; Zimmerli, L.; Koch, S.; Kawai, S.; Meyer, E. *Appl. Phys. Lett.* **2009**, *94*, 063303.
(50) Joachim, C.; Gimzewski, J. K. Aviram, a. *Nature* **2000**, *408*, 541–8.
(51) Venkataraman, L.; Klare, J.; Nuckolls, C.; Hybertsen, M.; Steigerwald, M. *arXiv Preprint cond-mat/0607836* **2006**, *442*, 1–4.
(52) Moth-Poulsen, K.; Bjø rnholm, T. *Nature nanotechnology* **2009**, *4*, 551–6.

(53) Zhong, D. Y.; Hirtz, M.; Wang, W. C.; Dou, R. F.; Chi, L. F.; Fuchs, H. *Phys. Rev. B* **2008**, *77*, 113404.
(54) Fendrich, M.; Kunstmann, T. *Appl. Phys. Lett.* **2007**, *91*, 023101.
(55) Tasker, P. W. *J. Phys. C: Solid State Phys.* **1979**, *12*, 4977.
(56) Shi, A.-C.; Wortis, M. *Phys. Rev. B* **1993**, *47*, 9804–9815.
(57) Bennewitz, R. *J. Phy.: Condens. Matter* **2006**, *18*, R417.
(58) Sugawara, A.; Hembree, G. G.; Scheinfein, M. R. *J. Appl. Phys.* **1997**, *82*, 5662–5669.
(59) Sugawara, A.; Mae, K. *J. Cryst. Growth* **2002**, *237*−*239*, 201–205.
(60) Repp, J.; Meyer, G.; Rieder, K.-H. *Phys. Rev. Lett.* **2004**, *92*, 036803.
(61) Zhang, Z. Y.; Lagally, M. G. *Science* **1997**, *276*, 377–383.
(62) Venables, J. A. *Introduction to Surface and Thin Film Processes*; Cambridge University Press: Cambridge U.K., 2000.
(63) Burton, W. K.; Cabrera, N.; Frank, F. C. *Philos. Trans. R. Soc. London, Ser. A - Math. Phys. Sci.* **1951**, *243*, 299–358.
(64) Mativetsky, J. M.; Miyahara, Y.; Fostner, S.; Burke, S. A.; Grutter, P. *Appl. Phys. Lett.* **2006**, *88*, 233121.
(65) Kawai, S.; Maier, S.; Koch, S.; Such, B.; Zimmerli, L.; Diederich, F.; Meyer, E. *Appl. Phys. Lett.* **2009**, 93–95.
(66) Bassett, G. *Philos. Mag.* **1958**, *3*, 1042–1045.
(67) Ruiz, R.; Choudhary, D.; Nickel, B.; Toccoli, T.; Chang, K.-C.; Mayer, A. C.; Clancy, P.; Blakely, J. M.; Headrick, R. L.; Iannotta, S.; Malliaras, G. G. *Chem. Mater.* **2004**, *16*, 4497–4508.
(68) Choudhary, D.; Clancy, P.; Shetty, R.; Escobedo, F. *Adv. Funct. Mater.* **2006**, *16*, 1768–1775.

JP107644U